

The Great Observatories Origins Deep Survey: Initial Results From Optical and Near-Infrared Imaging ¹

M. GIAVALISCO², H. C. FERGUSON^{2,12}, A. M. KOEKEMOER², M. DICKINSON^{2,12}, D. M. ALEXANDER³, F. E. BAUER³, J. BERGERON⁴, C. BIAGETTI², W. N. BRANDT³, S. CASERTANO², C. CESARSKY⁵, E. CHATZICHRISTOU⁶, C. CONSELICE⁷, S. CRISTIANI⁸, L. DA COSTA⁵, T. DAHLEN², D. DE MELLO⁹, P. EISENHARDT¹⁰, T. ERBEN¹⁹, S. M. FALL², C. FASSNACHT¹¹, R. FOSBURY^{14,17}, A. FRUCHTER², JONATHAN. P. GARDNER⁹, N. GROGIN¹², R. N. HOOK^{5,17}, A. E. HORNSCHEMEIER¹², R. IDZI¹², S. JOGEE², C. KRETCHMER¹², V. LAIDLER², K. S. LEE¹², M. LIVIO², R. LUCAS², P. MADAU¹³, B. MOBASHER^{2,14}, L. A. MOUSTAKAS², M. NONINO⁸, P. PADOVANI^{2,14}, C. PAPOVICH¹⁵, Y. PARK¹², S. RAVINDRANATH², A. RENZINI⁵, M. RICHARDSON², A. RIESS², P. ROSATI⁵, M. SCHIRMER^{18,19}, E. SCHREIER², R. S. SOMERVILLE², H. SPINRAD¹⁶, D. STERN¹⁰, M. STIAVELLI², L. STROLGER², C. M. URRY⁶, B. VANDAME⁵, R. WILLIAMS², C. WOLF²⁰

²*Space Telescope Science Institute, 3700 San Martin Dr., Baltimore, MD 21218*

³*Department of Astronomy and Astrophysics, Pennsylvania State University, 525 Davey Lab, State College, PA 16802*

⁴*Institut d'Astrophysique de Paris – CNRS, 98bis Boulevard Arago, F-75014, Paris, France*

⁵*European Southern Observatory, Karl-Schwarzschild-Strasse 2, D-85748 Garching bei München, Germany*

⁶*Department of Astronomy, Yale University, PO Box 208101, New Haven, CT 06520*

⁷*Palomar Observatory, California Institute of Technology, Mail Stop 105-24, Pasadena, CA 91125*

⁸*Istituto, Nazionale di Astrofisica, Osservatorio Astronomico di Trieste, via G.B. Tiepolo 11, Trieste, I-34131, Italy*

⁹*NASA Goddard Space Flight Center, Laboratory for Astronomy and Solar Physics, Code 681, Greenbelt, MD 20771*

¹⁰*Jet Propulsion Laboratory, California Institute of Technology, Mail Stop 169-506, Pasadena, CA 91109*

¹¹*Department of Physics, University of California, Davis, 1 Shields Ave. Davis, CA 95616*

¹²*Department of Physics and Astronomy, The Johns Hopkins University, 3400 N. Charles St., Baltimore, MD 21218–2686*

¹³*Department of Astronomy and Astrophysics, University of California, Santa Cruz, 1156 High Street, Santa Cruz, CA 95064*

¹⁴*European Space Agency, Space Telescope Division*

¹⁵*Steward Observatory, University of Arizona, 933 Cherry Ave., Tucson, AZ 85721–0065*

¹⁶*Department of Astronomy, University of California, Berkeley, Mail Code 3411, Berkeley, CA 94720*

¹⁷*Space Telescope European Coordinating Facility, European Southern Observatory, Karl–Schwarzschild–Strasse 2, D–85748 Garching bei München, Germany*

¹⁸*Institut für Astrophysik und Extraterrestrische Forschung, Universität Bonn, Auf dem Hügel 71, Bonn, Germany*

¹⁹*Max-Planck-Institut für Astrophysik, Karl–Schwarzschild–Strasse 1, D–85748 Garching bei München, Germany*

²⁰*Department of Physics, University of Oxford, Keble Road, Oxford, OX1 3RH*

ABSTRACT

This Special Issue of the *Astrophysical Journal Letters* is dedicated to presenting initial results from the Great Observatories Origins Deep Survey (GOODS) that are primarily, but not exclusively, based on multi-band imaging data obtained with the *Hubble Space Telescope* (*HST*) and the Advanced Camera for Surveys (ACS). The survey covers roughly 320 square arcminutes in the ACS F435W, F606W, F814W, and F850LP bands, divided into two well-studied fields. Existing deep observations from the *Chandra X-ray Observatory* (*CXO*) and ground-based facilities are supplemented with new, deep imaging in the optical and

¹Based on observations obtained with the NASA/ESA *Hubble Space Telescope* obtained at the Space Telescope Science Institute, which is operated by the Association of Universities for Research in Astronomy, Inc. (AURA) under NASA contract NAS 5-26555; observations collected at the European Southern Observatory, Chile (ESO Programmes 168.A-0845, 64.O-0643, 66.A-0572, 68.A-0544, 164.O-0561, 169.A-0725, 267.A-5729, 66.A-0451, 68.A-0375, 168.A-0485, 164.O-0561, 267.A-5729, 169.A-0725, 64.O-0621, 170.A-0788); observations collected at the Kitt Peak National Observatory, National Optical Astronomical Observatories, which is operated by AURA under cooperative agreement with the National Science Foundation.

near-infrared from the European Southern Observatory (ESO) and from the Kitt Peak National Observatory (KPNO). Deep observations with the *Space Infrared Telescope Facility* (SIRTF) are scheduled. Reduced data from all facilities are being released worldwide within three to six months of acquisition. Together, this data set provides two deep reference fields for studies of distant normal and active galaxies, supernovae, and faint stars in our own galaxy. This paper serves to outline the survey strategy and describe the specific data that have been used in the accompanying letters, summarizing the reduction procedures and sensitivity limits.

Subject headings: cosmology: observations — galaxies: formation — galaxies: evolution — galaxies: distances and redshifts

1. INTRODUCTION

Observations of representative fields at high galactic latitude have long been an important tool in our quest to understand the distant universe. The Hubble Deep Field project (Williams et al. 1996; 2000) demonstrated the value of deep, multicolor *HST* imaging for studies of galaxy evolution, and the extraordinary multiplier of this value gained by rapid public dissemination of the data and coordination of the best observations at all wavelengths on common survey fields (see Ferguson, Dickinson & Williams 2000 for a review). The Great Observatories Origins Deep Survey is the next generation of such deep surveys, uniting some of the deepest observations from space and ground-based facilities on common areas of the sky. The two GOODS fields, the Hubble Deep Field North (HDF-N) and the Chandra Deep Field South (CDF-S), are the most data-rich deep survey areas on the sky. The deepest X-ray observations from the *CXO* and *XMM-Newton* telescopes have been obtained at these locations, and deep radio maps are available or are now being collected. Observations with *SIRTF* were selected as one of the Legacy projects to be executed during the first year of the mission. The *SIRTF* Legacy project includes major commitments of observing time from the National Optical Astronomical Observatories (NOAO) and from the European Southern Observatory to provide spectroscopy (redshifts) for sources in the fields to the practical limits of existing instruments and to provide complementary imaging at near ultraviolet (*U*-band) and near infrared wavelengths. The GOODS project was subsequently awarded 398 orbits of time to observe the two fields with *HST* and ACS.

The GOODS project has been designed from the outset as a resource for the entire astronomical community. Data from the *HST* observations are available from the archive within a few days of the observations. Reduced data, with successive degrees of refinement,

are available within a few months of the observations. A similar strategy is followed for the ESO observations, and will be followed for *SIRTF*. The publicly released *HST* images have already been exploited by Stanway et al. (2003) and Bunker et al. (2003) to study galaxies at $z > 5$, and by Dawson et al. (2002) to study a hard X-ray emitting spiral galaxy. The ESO near-infrared images have been used by Roche et al. (2003) and Yan et al. (2003).

The GOODS field centers (J2000.0) are $12^{\text{h}}36^{\text{m}}55^{\text{s}}$, $+62^{\circ}14^{\text{m}}15^{\text{s}}$, for the HDF-N, and $3^{\text{h}}32^{\text{m}}30^{\text{s}}$, $-27^{\circ}48^{\text{m}}20^{\text{s}}$, for the CDF-S. Each field provides an area of approximately $10' \times 16'$ that will be in common to all the imaging observations. As of May 2003 the *CXO* data are all reduced and available, all of the *HST* data have been obtained and are available, including a best-effort version of the reduced data, while the recalibrated, mosaiced stacks of the ACS images will be released at the end of August. Much of the planned optical imaging data from KPNO and ESO have been obtained and are available. Deep near-IR imaging campaigns with the ESO Very Large Telescope (VLT) ISAAC camera and the KPNO FLAMINGOs camera are partially complete, but will require one or two more observing seasons for complete field coverage. Reduced data from first season (2001) of ISAAC observing are available. The planned spectroscopic campaign from ESO was begun in the Fall of 2002 with Focal Reducer/low-dispersion spectrograph (FORS2) observations of preferentially red objects. Observations with the VIMOS spectrograph are planned for the 2003-2004 CDF-S observing season. The HDF-N already benefits from deep spectroscopic observations from Cohen et al. 2000. Several teams are carrying out spectroscopic observations of the HDF-N from the W.M. Keck Observatory in early 2003, and public releases from a few of these teams are planned for the second half of this year.

The GOODS ACS observations were spaced in time to permit a search for type Ia supernovae at redshifts $z \approx 1.4$, and a total of 43 supernovae have been detected in eight GOODS search epochs. In their letter, Riess et al. provide details of how the type Ia candidates at $z > 1$ are selected for followup observations from among these sources. The other accompanying letters papers in this issue present initial findings on galaxies and AGN at moderate to very high redshifts from the analysis of the available GOODS data. A letter by Somerville et al. presents computations of the expected “cosmic variance” for various source populations based on halo statistics in Cold-Dark Matter models consistent with the Wilkinson Microwave Anisotropy Probe (WMAP) cosmological parameters (Spergel et al. 2003).

2. The Data Set

The data set discussed here includes ACS images, deep optical and near-infrared imaging from KPNO and ESO, and the *CXO* images. The main features of each data set are summarized in Table 1, while Table 2 lists the sensitivity achieved in each wavelength band. Figures 1 and 2 show the exposure maps of the three space-based data sets overlaid on top of each other to illustrate the extent of the area in common. Figure 3 shows a schematic of the layout of the existing imaging coverage in the CDF-S.

3. The HST ACS Data

The GOODS/ACS observations consist of imaging in the F435W, F606W, F775W and F850LP passbands, hereafter referred to as B_{435} , V_{606} , i_{775} and z_{850} . While the B_{435} -band images were all acquired at the beginning of the survey, the V_{606} , i_{775} , and z_{850} -band images have been carried out in five epochs, separated by 40 to 50 days to optimize the search for high-redshift supernovae. Only 60% of the total exposure time in each field (3 epochs out of 5) in the V_{606} , i_{775} , and z_{850} are presented here, since the remainder of the data were not available at the time these papers were being prepared. In the odd-numbered epochs each $10' \times 16'$ field is tiled by a grid of 3×5 individual ACS pointings, including some area of tile overlapping to check photometric and astrometric consistency. In even-numbered epochs, due to *HST* pointing constraints, the field is rotated by 45° and a different overlapping tiling pattern is used, consisting of 16 separate pointings (see Figures 1 and 2). The complete set of B_{435} observations were obtained in the first epoch alone, using the 3×5 grid, with six exposures per position.

The exposure times at each epoch are typically 1050, 1050 and 2100 seconds in the V_{606} , i_{775} and z_{850} bands, respectively. These are subdivided into 2 exposures in each of the V_{606} and i_{775} bands, and into 4 exposures in the z_{850} band. This strategy ensures good rejection of cosmic ray events in the single-epoch z_{850} bands, which is where the detection of transients is carried out. Some cosmic rays remain in the V_{606} and i_{775} single-epoch images, which can nevertheless generally provide colors of the transients. In each case, the telescope field of view is shifted (“dithered”) by a small amount between individual exposures to allow optimal sampling of the point-spread function and to remove detector gaps and artifacts. The multiple epochs are later combined into a single mosaic, allowing cosmic ray rejection from at least six images per band. Except for the B_{435} band, the mosaics used for the current papers were constructed from only three epochs of observations, and the total exposure times are approximately 7200, 3040, 3040, and 6280 seconds in the B_{435} , V_{606} , i_{775} , and z_{850} bands, respectively.

Basic reduction of the raw data is carried out through `calacs`, the ACS calibration pipeline, which applies the basic calibration steps of bias subtraction, gain correction, and flat-fielding (Pavlovsky et al. 2002). The data received from the *HST* pipeline are then further processed by the GOODS pipeline using the `multidrizzle` script (Koekemoer et al. 2003), to create a set of geometrically rectified, cosmic-ray cleaned images (within a given epoch). These processed “tiles” are released as the “best-effort” GOODS public release v0.5 via the Multimission Archive at Space Telescope (MAST).

The early version of the geometric distortion model used in the basic processing described above proved to have significant problems matching sources in overlapping tiles. To rectify this, we derived an astrometric solution for each tile and each epoch based on sources matched in GOODS groundbased images. The reference for the CDF-S image was the *R*-band image of the field obtained as part of the ESO Imaging Survey (EIS) with the Wide Field Imager (WFI), which in turn was astrometrically calibrated to the Guide Star Catalog 2 (GSC-2) and put on the ICRS reference frame. For HDF-N, the reference image was an *R*-band Subaru image of the field (Capak et al. 2003).

The astrometric solution for the *z*-band mosaics has been derived by a least-squares optimization of the position, orientation, *x* and *y* pixel scales, and axis skew of each tile and epoch, minimizing the inter-epoch variations of the estimated position for ~ 2000 sources. The estimated rms in the source position, internal to the solution, is about 0.1 to 0.2 WFC pixels. For the other ACS bands, the astrometric solution is based on a tile-by-tile match to *z*-band source positions. These solutions had a residual rms of about 0.3 pixels, with larger deviations in some local regions across the field. All the exposures were then drizzled (Fruchter & Hook 2002) onto a series of images with a common pixel grid, in order to create a clean median image, which was subsequently used to create a cosmic ray mask for each exposure. Finally, the individual exposures were drizzled, using the new masks, onto a final single mosaic for each band, measuring 18000 by 24000 pixels with a scale of $0''.05/\text{pixel}$.

For the purposes of the current papers the astrometric solution appears to be acceptable, although its deficiencies become apparent for bright stars, where the cosmic ray rejection algorithm rejects some good pixels due to the slight misregistrations. This can bias fluxes (faintward) for the brighter point sources in the V_{606} and i_{775} images (only). We have verified that there is little or no photometric effect for even slightly extended sources. A photometric comparison of the V_{606} magnitudes (SExtractor `MAG_AUTO` values) in the original WFPC-2 HDF-N and the current mosaic reveals systematic biases of less than 0.01 magnitudes for galaxies in the range $23 < V_{606} < 26$, with an rms scatter less than 0.2 mag.

The resulting mosaics have a few remaining blemishes and some misregistrations between bands at the level of a fraction of a pixel. Slight sky level variations are also apparent. The

masking of satellite trails, and reflection ghosts is not yet perfect, with residuals apparent in few places. The samples of galaxies used for the papers in this volume have all been individually inspected to remove objects that are thought to be artifacts. For most samples such contamination is negligible, but the contamination is significant for the single-band detections used to search for galaxies at $z \sim 6$, as discussed in detail by Dickinson et al. (2003).

4. The *CXO* Data

Chandra data in the GOODS fields were taken before the GOODS project began and are available from the *CXO* archive (Giacconi et al. 2002; Alexander et al. 2003). The integration times of the *Chandra* CDF–S and HDF–N observations total roughly 1 and 2 Msec, respectively. The GOODS *SIRTF* field layout was designed in part to maximize the coverage of the X–ray area. Subsequently, the ACS fields were designed to optimally cover both the *SIRTF* and *Chandra* fields. The *CXO* data for both fields have been re–analyzed in a self–consistent way, and new catalogs have been published by Alexander et al. (2003). Finally, these X–ray catalogs have been matched to the ACS catalogs by Koekemoer et al. (in preparation) for CDF–S and by Bauer et al. (in preparation) for HDF–N. Over 90% of the area covered by the GOODS ACS observations, the $S/N \geq 10$ point source sensitivity limits in the 0.5–2.0 keV and 2–8 keV bands, respectively, are 3.3 and 24×10^{-16} erg s $^{-1}$ cm $^{-2}$ for the HDF–N and 4.3 and 30×10^{-16} erg s $^{-1}$ cm $^{-2}$ for the CDF–S. The sensitivities at the *CXO* aim point, where the exposure time and image quality are maximized, are as much as a factor of ~ 2 and ~ 4 fainter for the CDF–S and HDF–N, respectively.

5. Ground–based Near–UV, Optical, and Near–IR Imaging

Ground–based imaging spanning a wide wavelength baseline is an important component of GOODS, and here, we describe the data that have been used for projects presented in this Special Issue. The CDF–S imaging consists of a complex arrangement of data sets covering different areas, often using multiple instrument pointings, as illustrated in Figure 3. These data sets were all placed on a common astrometric grid tied to the GSC2. The PSFs were matched by Gaussian convolution to a common FWHM of $0''.9$. The WFI *U'UBV* images and a few of the images obtained with the New Technology Telescope (NTT) and the Superb–Seeing Imager (SOFI) have slightly poorer seeing, $0''.9$ – $1''.05$, but most projects use colors measured through $3''$ apertures, so this small mismatch should have little effect. The PSF–matched images were mosaiced onto a common $0''.3$ pixel grid with the SWarp software

(Bertin 2002). Noise maps were constructed for use in object detection and cataloging, carefully accounting for the effects of interpixel correlations. High-resolution ($0''.15/\text{pixel}$) ISAAC mosaics were also made without degrading their excellent image quality. We have used the colors of stars to check the photometric zeropoints of the CDF-S data, as described below. Where possible, these were identified using the ACS imaging, using criteria for star-galaxy separation based on a diagram of peak surface brightness vs. isophotal magnitude. The same method was used on the ground-based data to extend the stellar sample to areas beyond the ACS coverage.

5.1. KPNO 4m + MOSAIC *U*-band imaging

Deep *U*-band images of the GOODS HDF-N field were obtained using the prime focus MOSAIC camera on the KPNO Mayall 4-m telescope in March 2002. A total of 27.5 hours of exposure time were obtained in photometric conditions with mean seeing $\text{FWHM} = 1''.15$. We reduced the data using the IRAF `mscred` package, which carries out bias subtraction, flat-fielding, correction for geometric distortion, removal of amplifier cross-talk, subtraction of an additive “pupil ghost”, image registration, and combination.

5.2. ESO-MPI 2.2-m + WFI imaging

An area of ~ 0.4 sq. degree around the CDF-S was surveyed with WFI on the ESO-MPI 2.2-m telescope using the *UUBVRI* passbands. Much of these data were obtained as part of the EIS, and are described in Arnouts et al. 2001. Additional *BVR* images were obtained for the GOODS program and in the course of the COMBO-17 project (Wolf et al. 2001). The EIS, GOODS, and COMBO data were reduced in a uniform fashion using the GaBoDs WFI reduction pipeline (Schirmer et al. 2003). We carefully checked the accuracy of the photometric calibration using the color loci of stars. These were compared to synthetic color-color diagrams generated using the Gunn & Stryker (1983) spectrophotometric library, convolved with the instrumental passbands. Zeropoints were adjusted as necessary, and are accurate to < 0.1 mag.

5.3. ESO VLT + FORS1 imaging

Additional, deep *R* and *I*-band images were obtained with the ANTU telescope (UT1) at the VLT, using the FORS1 instrument. The data and their reduction are described in

Tozzi et al. (2001). The FORS1 images cover only a portion of the GOODS CDF–S field using several pointings with variable exposure time. A portion of the field is covered by relatively short R -band exposures. The core region ($13'.6 \times 13'.6$) is quite deep, however, and in particular is much deeper than the WFI imaging in the I -band. The photometric zeropoints were checked and adjusted by comparing photometry for stars and galaxies in the WFI and FORS1 images, accounting for the passband differences, and agree on average to < 0.05 mag.

5.4. ESO NTT + SOFI imaging

Near-infrared data in the J and K_s bands for the CDF–S were obtained with SOFI on the NTT as part of the EIS. The observations and reductions are described in Vandame et al. 2001. They consist of a 4×4 grid of pointings covering 0.1 sq. deg. SOFI H -band data were obtained and reduced by Moy et al. 2002, and cover a larger area. Photometric zero-points were checked by comparing photometry of stars to measurements from the Two-Micron All-Sky Survey (2MASS).

5.5. ESO VLT + ISAAC imaging

The GOODS program is gathering a mosaic of very deep JHK_s images with ISAAC on the VLT as part of an ESO Large Programme. Ultimately, 32 pointings will be used to cover the GOODS CDF–S field. Data for 8 fields were obtained in 2001–2 and combined with ISAAC data from an ESO visitor program, kindly provided by E. Giallongo. These images cover only ~ 50 arcmin², but are much deeper than the SOFI data, with excellent image quality (mean FWHM $\approx 0''.45$). They were reduced with the EIS pipeline. Their photometric zeropoints were adjusted to a common scale by comparison to objects in the SOFI images, and agree within 0.07 mag.

6. Source Catalogs

Several different source catalogs for the ACS and ground-based images are used in the accompanying papers. In all cases, source identification and photometry were performed using SExtractor (Bertin & Arnouts 1996). Simulations were used to guide the choice of detection thresholds and the size and shape of the convolution kernel to optimize the detection of faint galaxies while keeping spurious sources to a minimum. Photometric uncertainties

within any aperture are computed using the normalized noise maps that were produced as part of the data reduction process. However, some projects use detailed simulations with artificial sources to assess the true photometric errors.

For the ACS catalog, sources were detected in the z_{850} mosaic, and photometry was carried out through matched apertures in the other ACS bands. Several different ground-based catalogs were generated for the CDF-S, with detections based on the WFI R -band, SOFI K -band, and ISAAC K and J -bands. In each case, matched aperture photometry was measured for all of the other CDF-S ground-based images. A wide-field HDF-N catalog, based on Subaru $BVRIZ$ imaging and the GOODS KPNO U data, is presented by Capak et al. 2003, but is not used in the present set of Letters. Where needed, ACS-to-ground-based colors were measured using images degraded to match the ground-based PSFs. These provide optical-IR colors of ACS sources, as well as $U - B_{435}$ colors for Lyman break color selection.

Photometric redshifts for galaxies in the CDF-S (Mobasher et al. 2003) were estimated using all of the available photometry (U through K_s bands) and the BPZ software of Benítez (2000). They were tested against spectroscopic redshifts from the K20 survey (Cimatti et al. 2002), kindly provided by A. Cimatti, and also against redshifts measured with VLT+FORIS2 for the GOODS program.

7. Sensitivity

The sensitivity of the images depends on the sizes and shapes of the objects of interest. To guide the readers of these Letters, Table 2 provides two sensitivity estimates (point source flux and limiting surface brightness) for each of the GOODS space- and ground-based imaging data sets. These should be taken as representative values only, since the actual depths of the imaging data sets vary over the field of view, and depend on the details of source size, PSF shape, crowding, etc.

Many of the papers in this issue rely on SExtractor detections in the ACS z_{850} -band image. To assess the completeness limits for this catalog, we have iteratively inserted sources into the image and re-run SExtractor. This is the standard procedure used for point-source photometry to assess completeness and photometric errors in color-magnitude diagrams. The problem has more dimensions for galaxy photometry because the detectability of a galaxy depends on the size and surface brightness profile. Our simulations uniformly populate the magnitude range $20 < z_{850} < 28$ and the range of galaxy half-light radii $0''.01 < r < 1''.5$. The input galaxies are a 50/50 mix of spheroids — galaxies with $r^{1/4}$ -law surface-brightness

profiles — and disks with exponential surface-brightness profiles. The spheroids are assumed to be oblate and optically thin with an intrinsic axial ratio distribution that is uniform in the range $0.3 < b/a < 0.9$. The disks are modeled as optically-thin oblate spheroids with a (very flat) intrinsic axial ratio of $b/a = 0.05$. Galaxies are viewed from random inclinations. The simulated galaxies are convolved with the PSF and inserted into the z -band image without additional Poisson noise. For bright sources, the noise is thus slightly underestimated, but for faint sources, the sky background completely dominates anyway so this shortcut does not affect the results. The resulting completeness limits in a plane of magnitude and half-light radius are shown in Fig. 4.

8. Summary

The intent of this paper has been to provide a brief overview of the GOODS project and to describe the data used to derive the scientific results discussed elsewhere in this issue. The GOODS web site, which can be accessed from <http://www.stsci.edu/ftp/science/goods/>, provides further details of the project and access to the GOODS data.

Support for the GOODS *HST* Treasury program was provided by NASA through grants HST-GO09425.01-A and HST-GO-09583.01. Additional support for this work, which is also part of the *Space Infrared Telescope Facility (SIRTF)* Legacy Science Program, was provided by NASA through Contract Number 1224666 issued by the Jet Propulsion Laboratory, California Institute of Technology under NASA contract 1407. PM acknowledges support by NASA through grant NAG5-11513.

A project of the scale and scope of GOODS could not succeed without the dedicated efforts of a large number of people. We wish to thank Beth Perriello, Bill Workman, Ian Jordan, Denise Taylor and David Soderblom for their efforts in planning and scheduling the GOODS ACS observations. Guido De Marchi provided expert assistance on ACS issues. Dorothy Fraquelli and the OPUS group at STScI were instrumental in enabling the rapid turnaround of the data for the supernova search. Mark Calvin, Matt Divens, and the computer support group went well beyond the call of duty in their support of the data-reduction computers, on several occasions rescuing the supernova searches from impending disaster. We acknowledge the contributions of Len Cowie to the GOODS project, and thank Peter Capak for providing the Subaru optical catalog in advance of publication and helping to support the HDF-N supernova searches. We thank Emmanuel Moy, Dimitra Rigopoulou and Pauline Barmby for providing the SOFI H -images prior to publication, Emanuele Giallongo for contributing his ISAAC imaging of the CDF-S to the GOODS public-release data set,

and Andrea Cimatti and the K20 team for providing spectroscopic redshifts that were used to validate our photometric redshift estimates.

REFERENCES

- Alexander, D., et al., 2003, AJ, in press, astro-ph/0304392
- Arnouts, S., et al., 2001, A&A, 379, 740
- Benítez, N., 2000, ApJ, 536, 571
- Bertin, E., 2002, SWarp User’s Guide
- Bertin, E., and Arnouts, S., 1996, A&A, 117, 393
- Bunker, A., Smith, J., Spinrad, H., Stern, D. & Warren, S., 2003, astro-ph/0303290.
- Capak, P., et al., 2003, ApJ, submitted
- Cimatti, A., et al., 2002, A&A, 392, 395
- Cohen, J., Hogg, D. W., Blandford, R., Cowie, L. L., Hu, E. Songaila, A., Shopbell, P. & Richberg, K., 2000, ApJ, 538, 29
- Dawson, S., McCrady, N., Stern, D., Eckart, M., Spinrad, H., Liu, M., & Graham, J. R., 2002, astro-ph/0212240
- Dickinson, M., et al., 2003, this volume.
- Ferguson, H. C., Dickinson, M., & Williams, 2000, ARAA, 38, 667
- Fruchter, A. S. & Hook, R. N. 2002, PASP 114, 144
- Giacconi, R. et al., 2002, ApJS, 139, 369
- Gunn, J., & Stryker, 1983, ApJS, 52, 121
- Koekemoer, A. M., Fruchter, A. S. Hack, W. & Hook, R. N. 2003, *HST* Calibration Workshop (STScI: Baltimore)
- Madau, P., Pozzetti, L., & Dickinson, M. E. 1998, ApJ, 498, 106
- Mobasher, B., et al., this volume
- Moy E., et al. 2002, astro-ph/0211247
- Oke, J. B. 1974, ApJS, 27, 21
- Pavlovsky, C., et al. 2002, ACS Instrument Handbook, Version 3.0, (Baltimore: STScI).
- Riess, A., et al., 2003, this volume
- Roche, N., Dunlop, J. & Almaini, O., 2003, astro-ph/0303206

- Schirmer, M., Erben, T., Schneider, P., Pietrzynski, G., Gieren, W., Micol, A., Pierfederici, F. 2003, astro-ph/0305172
- Somerville, R. S., et al., 2003, this volume
- Spergel, D., et al., 2003, ApJ, submitted
- Stanway, E., Bunker, A., & McMahon, R., 2003, astro-ph/0302212
- Steidel, C. C., Giavalisco, M., Pettini, M., Dickinson, M., & Adelberger, K. 1996, ApJ,
- Tozzi, P., et al., 2001, ApJ, 562, 42
- Vandame, B., et al., 2001, A&A, submitted (astro-ph/0102300),
- Williams, R. E. et al. 1996, AJ, 112, 1335
- Williams, R. E. et al. 2000, AJ, 120, 2735
- Wolf, C., Dye, S., Kleinheinrich, M., Meisenheimer, K., Rix, H.-W., & Wisotzki, L., 2001, A&A, 377, 442
- Yan, H., Windhorst, R. A., Röttgering, H. J., Cohen, S. H., Odewhan, S. C., Chapman, S. C. & Keel, W. C., 2003, ApJ, 585, 67

Table 1. The Data

Facility	Passbands	Area coverage ^a	Angular resolution ^b	Field
<i>HST</i> + ACS	<i>BViz</i>	320 ^c	0.125 ^d	HDF-N + CDF-S
<i>CXO</i> + ACIS	0.5-8 keV	450 ^e	0.85–10 ^f	HDF-N
<i>CXO</i> + ACIS	0.5-8 keV	390 ^e	0.85–10 ^f	CDF-S
KPNO 4-m + MOSAIC	<i>U</i>	1800	1.15	HDF-N
ESO 2.2-m + WFI	<i>U'UBVRI</i>	>1350	0.85–1.05	CDF-S
ESO VLT + FORS1	<i>RI</i>	175 ^g	0.6–0.8	CDF-S
ESO NTT + SOFI	<i>JK_s</i>	360	0.65–1.05	CDF-S
ESO NTT + SOFI	<i>H</i>	630	0.55–0.85	CDF-S
ESO VLT + ISAAC	<i>JHK_s</i>	50	0.40–0.65	CDF-S

^aTotal area covered, in arcmin².

^bPSF FWHM, in arcseconds

^cArea with 4-band ACS coverage. The total area with *Viz*-band coverage is 365 arcmin².

^dModal PSF FWHM of current version of drizzled image mosaics. The intrinsic image quality of *HST*/ACS is better; future rereductions will improve the net image quality.

^eTotal *CXO* coverage. Exposure time and PSF, and hence net sensitivity, are a strong function of area.

^f*CXO* PSF quoted as 50% encircled energy diameter, from on-axis to the maximum off-axis angle within the GOODS ACS area.

^gDeep area only. The FORS *R* mosaic covers an additional 160' at shallower depth.

Table 2. Sensitivity for Current GOODS Optical and Near-Infrared Data

Facility	U'	U	B	V	R	I	z	J	H	K_s
<i>HST</i> +ACS	27.8	27.8	...	27.1	26.6
<i>HST</i> +ACS	28.4	28.4	...	27.7	27.3
4-m MOSAIC	...	25.9
4-m MOSAIC	...	29.0
2.2-m WFI	25.0 ^a	24.7 ^a	26.2	25.8	25.8	23.5
2.2-m WFI	28.1 ^a	27.9 ^a	29.3	28.9	28.9	26.6
VLT FORS1	26.2	25.9
VLT FORS1	29.4	29.0
NTT SOFI	22.8	22.0	21.8
NTT SOFI	25.9	25.1	25.0
VLT ISAAC	25.5	24.9	25.1
VLT ISAAC	27.9	27.3	27.4

For each telescope + instrument combination, the first line gives the 10σ point-source sensitivity within an aperture diameter of $0''.2$ for *HST*, $1''.0$ for ISAAC, and $2''.0$ for other ground-based data. The second line gives the 1σ surface brightness fluctuations in an aperture with area 1 arcsec^2 . The values reported are medians over the area covered by the *HST*/ACS imaging, except for the FORS1 R data which is a value for the area covered by the deeper portion of the data. Units in AB mag (Oke 1974) and AB mag arcsec⁻², respectively.

^aThe WFI U -band is highly non-standard (see Arnouts et al. 2001). The so-called U' filter for WFI is closer to a standard U passband.

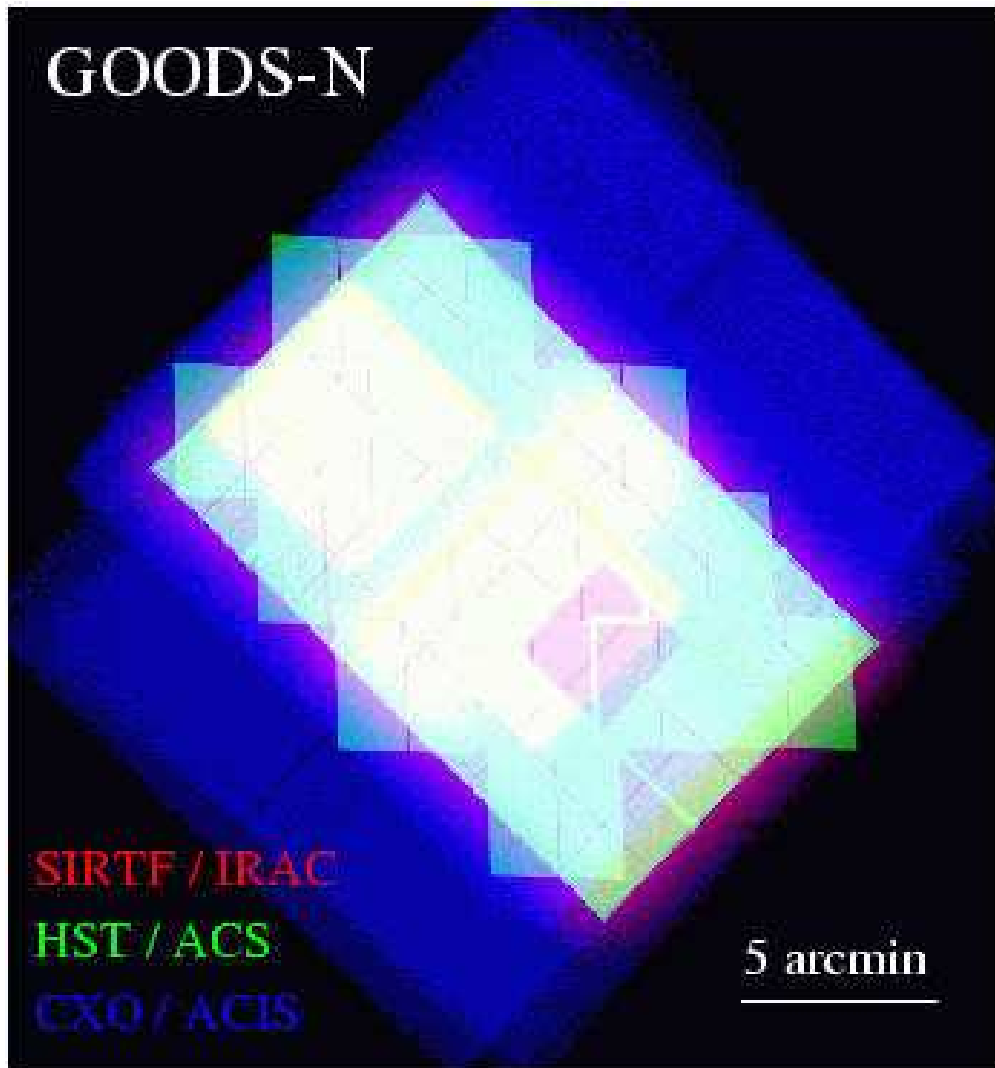


Fig. 1.— Exposure map of the GOODS HDF-N Observations. In this image, blue represents the *Chandra* (*CXO*) exposure map for the 2 Msec observations described by Alexander et al. (2003). Green represents the current *HST/ACS* exposure map, and red represents the planned *SIRTf/IRAC* exposure map. Where all fields overlap, the colors sum to give white in the representation. The different ACS tiling patterns on even and odd epochs produce the sawtooth pattern around the edge of the ACS fields. A guide-star failure on one of the ACS tiles produces the reddish square seen within the ACS rectangle. This exposure will be repeated to even out the final exposure map. The two planned 75-hour IRAC ultra-deep fields can be seen faintly within the ACS area. These ultra-deep fields are planned only for the HDF-N.

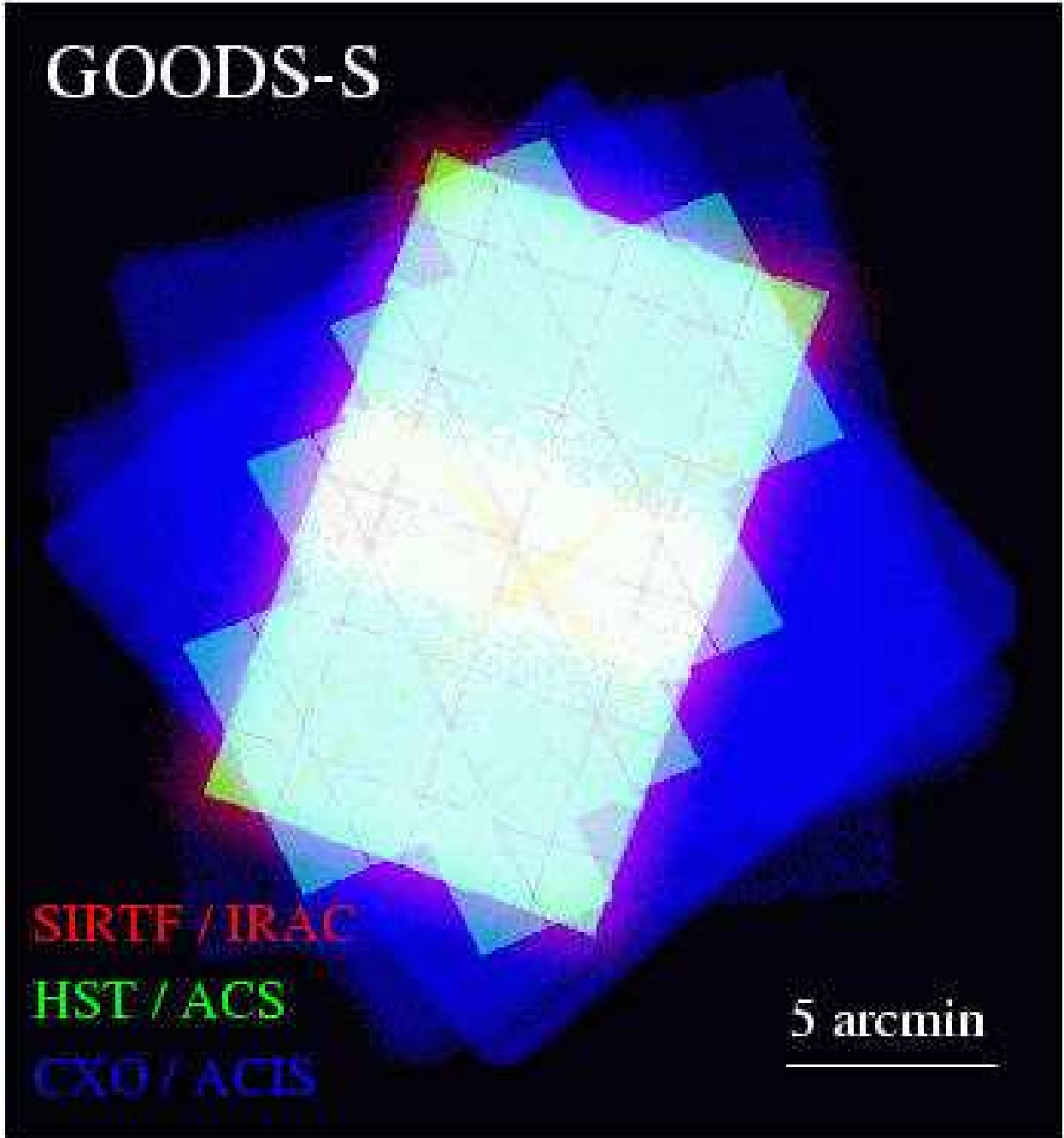


Fig. 2.— Exposure map of the GOODS CDF-S Observations. The color-map is the same as for Fig. 1. The *Chandra* observations are those of Giacconi et al. (2002).

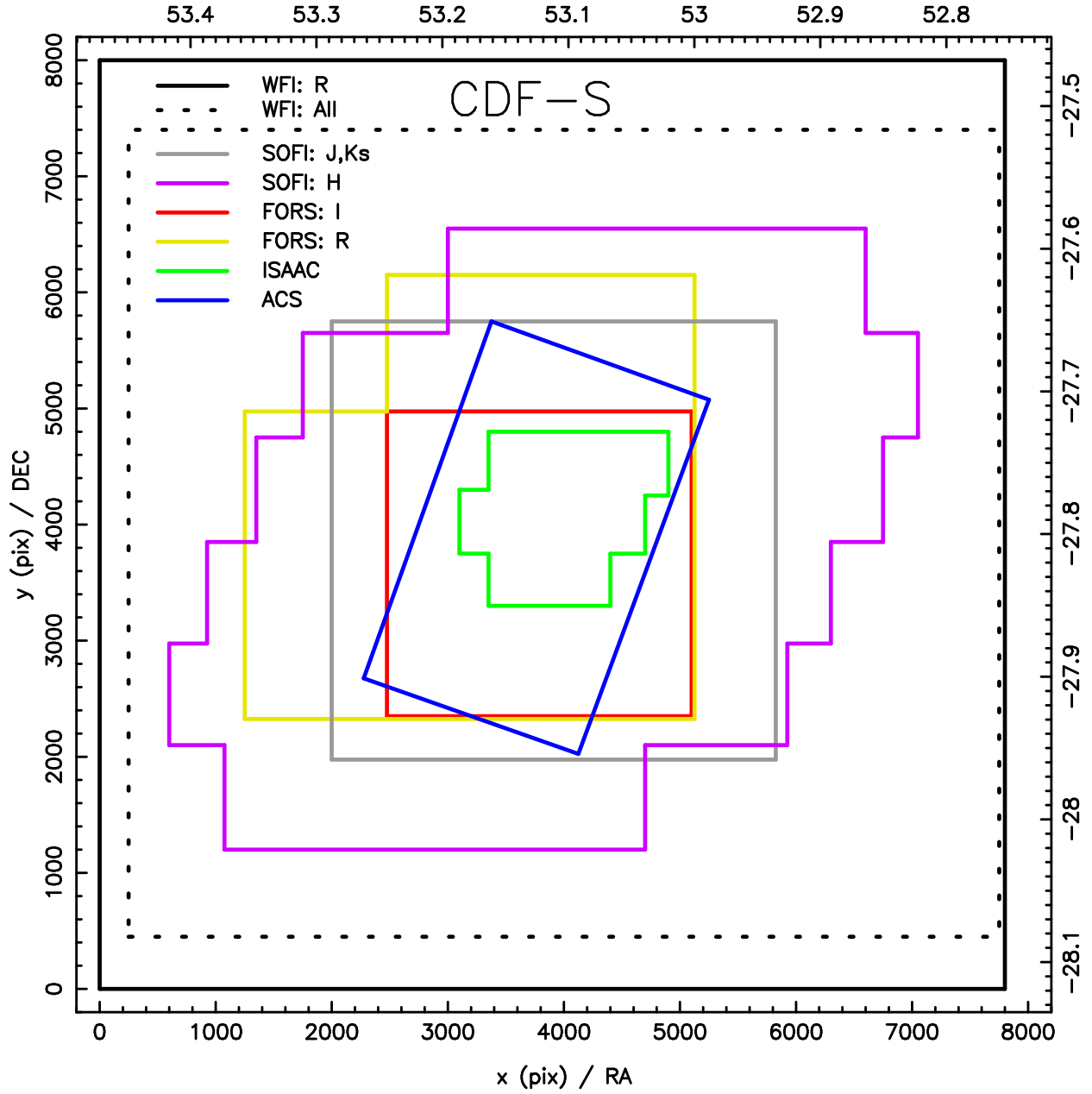


Fig. 3.— Schematic outline of the GOODS data sets in the CDF-S region. The blue shows the outline of the ACS area. The other colors outline the areas covered by the ESO data described in the text.

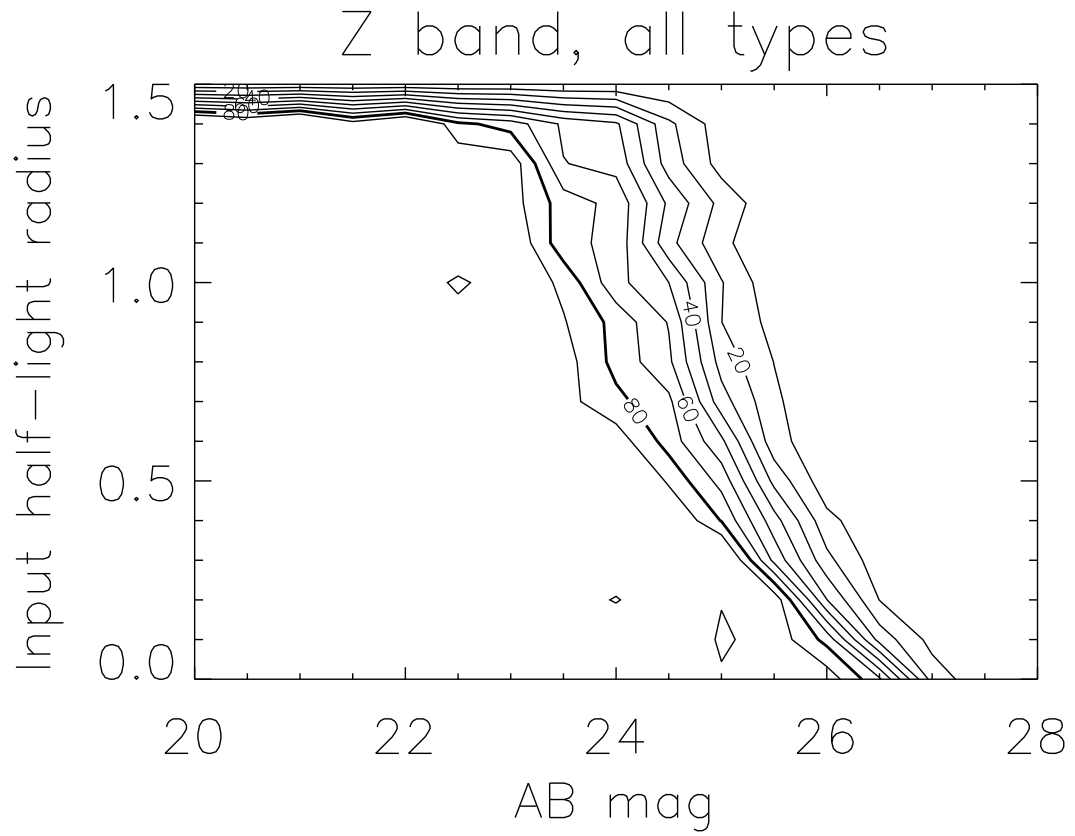


Fig. 4.— Completeness limits for the GOODS ACS z -band catalog as a function of galaxy total magnitude and half-light radius. The contours show the percentage of galaxies recovered by SExtractor in the simulations described in the text.